LIMNOLOGY and OCEANOGRAPHY

ASLO

Limnol. Oceanogr. 71, 2026, e70418

doi: 10.1002/lno.70418

RESEARCH ARTICLE

The contrasting effects of vegetation height and density on flow and turbulence in a patch of vegetation

Masaya Yoshikai [1,2*] **Julia C. Mullarney,** [1] **Vinay Nelli** [1] **Rémi Chassagne,** [1,3] **William Nardin,** [4] **Rafael O. Tinoco** [5]

[1]Coastal Marine Group, School of Science, University of Waikato, Hamilton, New Zealand; [2]School of Engineering, University of Waikato, Hamilton, New Zealand; [3]Université Grenoble Alpes, LEGI CNRS UMR, Grenoble, France; [4]Horn Point Laboratory, University of Maryland Center for Environmental Science, Cambridge, Maryland, USA; [5]Department of Civil and Environmental Engineering, University of Illinois Urbana, Champaign, Illinois, USA

Abstract

Coastal vegetation often grows in spatially distributed patches. However, the influence of individual vegetation patches on small-scale hydrodynamics has not been well characterized under natural conditions with tidally varying water depths. We present measurements from manipulative field experiments by creating artificial patches of vegetation mimics with different patch heights and densities. We found that increased vegetation density substantially reduces flow speeds and turbulent kinetic energy (TKE) within the patch. However, for submerged patches, an increase in vegetation height induced a contrasting effect, causing faster flows and greater TKE within the patch, despite an increase in the total vegetation frontal area exerting drag. Denser patches showed the same, although more pronounced, trend. Existing analytical models failed to accurately reproduce both the observed patterns and magnitudes in velocity and TKE as functions of vegetation height and density. In contrast, the corresponding numerical hydrodynamic simulations captured both patterns and magnitudes well. These results underscore the need to correctly account for such opposing effects of vegetation geometries on flow and turbulence, and hence on sediment transport when predicting geomorphic evolution in coastal vegetation habitats.

Coastal vegetation, such as mangroves and salt marshes, grows in intertidal zones. The presence of stems or aboveground roots is known to significantly alter water flow by exerting drag (Nepf 2012; Horstman et al. 2021; Yoshikai, Nakamura, Suwa, Argamosa, et al. 2021) and creating stem-scale turbulence (Norris et al. 2017), thus changing sediment transport (Furukawa et al. 1997; Mudd et al. 2010) and driving long-term geomorphic change (Mariotti and Fagherazzi 2010; Fagherazzi et al. 2012; Nardin et al. 2016). In some cases, the sediment trapping can occur at a sufficient rate that the elevation of these habitats can keep pace with sea-level rise (Mariotti 2020; Cai et al. 2022; Belliard et al. 2023). A better understanding of flow and sediment transport in vegetated regions is therefore critical for assessing the persistence of coastal vegetation in the face of climate change.

To date, laboratory and numerical studies have extensively examined mean flows and turbulent kinetic energy (TKE) in vegetated regions, for both emergent (e.g., Nepf 1999; D. Liu et al. 2008; Etminan et al. 2017) and submerged vegetation (e.g., Nepf and Vivoni 2000; Ghisalberti and Nepf 2004), by using arrays of vertical cylinders mimicking vegetation. These studies focused on fully developed flows assuming wide (in longitudinal and lateral directions) and homogeneous vegetation canopies; however, coastal vegetation often occurs in patches (Balke et al. 2012; Bouma et al. 2013; Dai et al. 2021). Previous studies on patches of emergent vegetation have shown that flow is deflected around a patch, causing fast flow velocities at the sides of the patch and slow velocity within (Vandenbruwaene et al. 2011; Z. Chen et al. 2012; Zong and Nepf 2012). Thus, heterogeneity of vegetation can shape different landscapes, compared to those formed in cases with homogeneous vegetation (Schwarz et al. 2018, 2022; da Silva et al. 2024). In contrast, insights into flow and turbulence in

*Correspondence: masaya.yoshikai@waikato.ac.nz

Associate editor: Ruth Reef

patches of submerged vegetation are rather limited. Submerged vegetation patches deflect flow at the sides and above the patch (Ortiz et al. 2013; M. Liu et al. 2021; Cornacchia et al. 2022), imposing additional complexities to the case of emergent vegetation patches. Recently, Lei and Nepf (2021) used results from a laboratory study to develop a predictive model for flow velocity in a submerged vegetation patch. They hypothesized that the water-depth dependence of flow velocity in the patch will diminish under field conditions because majority of water flow will be deflected at the unbounded sides of the patch. However, this hypothesis has not been well verified.

Moreover, flume studies may not extrapolate well to the real-world conditions (Tinoco et al. 2020). First, it is challenging to control both velocity and water depth in a flume, limiting the number of water depths (or vegetation submergence ratio) for examination (Tinoco et al. 2020). Second, it is challenging to eliminate the side-wall effects given the typical scale of laboratory flumes. Contrastingly, in nature, flows are unbounded by side-walls and flow velocity and water depth are continuously changing, so that coastal vegetation such as pneumatophores of *Avicennia* mangroves (cylindrical-shaped areal roots) experience transitions from emergence to submergence regime every tidal cycle (Y. Chen et al. 2016; Bryan et al. 2017; Mullarney, Henderson, Norris, et al. 2017). Therefore, these conditions leave a key knowledge gap in real-world conditions of flow and turbulence in patchy coastal vegetation.

To address these knowledge gaps, we conducted manipulative experiments in the field by creating artificial patches of vegetation mimics to control vegetation parameters while retaining natural forcing conditions, thereby extending insights from laboratory to the field. We examined the effects of two primary vegetation parameters—patch density and height (Nepf et al. 2007; Mullarney and Henderson 2018), on mean velocity and near-bed TKE—a regulator of sediment resuspension and bedload transport (Diplas et al. 2008; Salim et al. 2017; Yang and Nepf 2018). We specifically test (1) if a model to predict near-bed TKE in fully developed vegetated flows proposed by previous studies applies to flows in a vegetation patch under field conditions and (2) if there is no dependence of flow on water depth as hypothesized by Lei and Nepf (2021). Here, through observations under field conditions, we characterize the contrasting effects of vegetation density and height over a smoothly changing water depth. We additionally perform numerical simulations to complement our findings from the field.

Materials and methods

Field experiments

The field experiments were conducted on an intertidal sand flat in Purangi Estuary, New Zealand (36.842°S, 175.759°E; Fig. 1a). The tide is semi-diurnal with water depths up to ~ 0.75 m at high tide (Nelli et al. 2026). Patchy young *Avicennia marina* mangroves grow at ~ 50 m away from the experiment site (Supporting Information Fig. S1), sufficient distance to avoid the influence of those trees on our experiment. The median grain diameter of the sediments is 185 μm, which was determined using a particle size analyzer (Malvern Instruments) on surface grab samples from the sand flat.

We conducted two sets of experiments with different vegetation heights (h_{veg}): Experiment 1 for $h_{veg} = 0.1$ m (August 29, 2023 to September 1, 2023) and Experiment 2 for $h_{veg} = 0.2$ m (September 26, 2023 to September 29, 2023). In each experiment, we created three 1-m diameter circular patches of vegetation mimics (5-mm diameter bamboo dowels) with equal spacing between neighboring dowels distributed in a staggered pattern. We tested three vegetation densities: dense (1500 m^{-2}), intermediate (500 m^{-2}), and sparse (125 m^{-2}) (Fig. 1c–e). Geometrical features are based on ranges of reported geometry of pneumatophores of *Avicennia* spp. stands (Dahdouh-Guebas et al. 2007; Vovides et al. 2016; Yoshikai, Nakamura, Suwa, Rollon, et al. 2021). Table 1 summarizes the key geometric and drag-related parameters for the patches.

We conducted high-frequency (50-Hz sampling rate) velocity measurements close to the center of a patch using three Profiling Acoustic Doppler Velocimeters—Nortek Vectrino Profilers (VPs; Fig. 1c–e), with VP1 positioned to measure flow profiles at approximately 0.02–0.05 m above the bed, and VP2 and VP3 at approximately 0.01–0.04 and 0.12–0.15 m above the top of the vegetation, respectively, with 1-mm vertical bins. Measurements were conducted for two tidal cycles for each patch density.

We deployed several Acoustic Doppler Current Profilers (ADCPs)—Nortek Signature, Nortek 2 MHz Aquadopps—and Acoustic Doppler Velocimeters—Nortek Vectors—to characterize flow (velocities and pressure) in the vicinity of the patches (Fig. 1b). The Vectors were deployed behind and in front of the patches during flood and ebb tides, respectively. The measurement location was approximately $2h_{veg}$ away from the edge of the patches, and the patch centerline extending to the instrument head was approximately aligned with the direction of tidal flows (Fig. 1b). The Vectors were positioned to measure three components of velocities at 0.05 m above the bed with a 32 Hz sampling rate. The ADCPs were deployed looking upwards. The Aquadopps used pulse-coherent mode to measure short (0.5 m) velocity profiles with 0.025-m vertical bins at 8 Hz sampling rate. The Signature measured velocities with 0.02-m vertical bins over the full water column at 4 Hz. In addition, the atmospheric pressure was measured using a HOBO U20L-04.

Post-processing of VP data

The data from VPs were processed to remove low-quality data (correlations < 50%, signal-to-noise ratio < 10 dB), and the data gaps were filled by polynomial interpolation. The

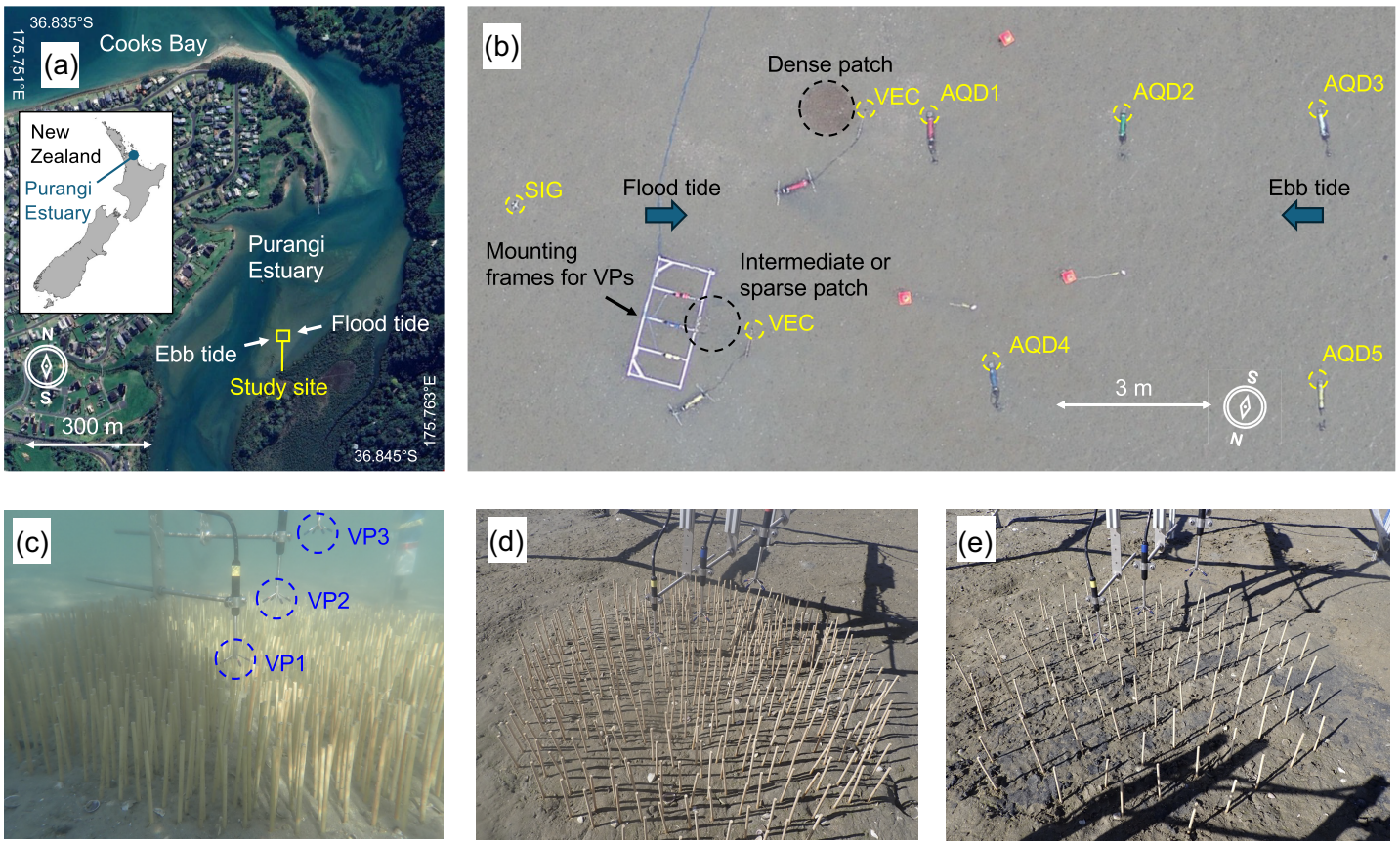

Fig. 1. (**a**) Location of study—Purangi Estuary in Coromandel Peninsula, Waikato, New Zealand (yellow box indicates site of experiment); (**b**) drone photograph of the experiment site with vegetation patches and deployed instruments during Experiment 1; photos of the (**c**) dense, (**d**) intermediate, and (**e**) sparse patches with Nortek Vectrino Profilers (VPs) positioned to measure flows within the patch (VP1), at the top of the vegetation mimics (VP2), and above the vegetation (VP3). AQD, Nortek Aquadopp; SIG, Nortek Signature; VEC, Nortek Vector.

Table 1. Geometric and drag-related parameters of vegetation mimics. h_{veg} is vegetation height, n_{veg} is vegetation density, a is the frontal area density of the patch, ϕ is the solid volume fraction of the patch, δ is the penetration length in a fully developed condition, defined as the depth that the shear layer vortices penetrate into the canopy. X_{2D} is the adjustment length estimated for two dimensional (2D) canopies using Eq. 4 for water depths of 0.2–0.8 m when $h_{veg} = 0.1$ m, and for water depths of 0.3–0.8 m when $h_{veg} = 0.2$ m. X_{3D} is the adjustment length estimated for three dimensional (3D) canopies using Eq. 7 (no dependence on water depth). $C_D a h_{veg}$ represents the momentum absorption capacity of the canopy, where C_D (= 1.0) is the drag coefficient. The values of δ are the ranges estimated from $\delta = \min\left(\frac{0.3 \pm 0.1}{C_D a}, h_{veg}\right)$ based on Lei and Nepf (2021).

Experiment	Patch	h_{veg} (m)	n_{veg} (num m^{-2})	a (m^{-1})	ϕ	$C_D a h_{veg}$	δ (m)	X_{2D} (m)	X_{3D} (m)
1	Dense	0.1	1500	7.5	0.029	0.75	0.03–0.05	0.42–0.59	0.34
1	Intermediate	0.1	500	2.5	0.010	0.25	0.08–0.10	1.09–1.26	1.01
1	Sparse	0.1	125	0.625	0.002	0.0625	0.1	4.09–4.26	4.01
2	Dense	0.2	1500	7.5	0.029	1.5	0.03–0.05	0.64–0.94	0.34
2	Intermediate	0.2	500	2.5	0.010	0.5	0.08–0.16	1.31–1.61	1.01
2	Sparse	0.2	125	0.625	0.002	0.125	0.2	4.31–4.61	4.01

instantaneous velocity data were then despiked using the phase-space method described in Goring and Nikora (2002) and Mori et al. (2007). We applied a low-pass filter with a cut-off period of 1 min to remove velocity fluctuations that are not likely attributed to turbulence. The processed velocities were then segmented into 5-min windows. On-site observations and the spectra of velocities and water depths suggested the occasional presence of small wind waves, especially during

Experiment 2 (significant wave height, $H_s < 0.05$ m, but 80% of the time $H_s < 0.01$ m). In order to extract the turbulent component from the velocity fluctuations, we applied the wave-turbulence decomposition of Bricker and Monismith (2007) for each 5-min segment.

The velocity components u, v, and w correspond to the streamwise (x), lateral (y), and vertical (z, where $z = 0$ at the bed) directions, respectively. Note that the orientation of x and y axes were adjusted for each 5-min segment based on the mean flow direction measured by an ADCP upstream from the patches. Time-averaged streamwise velocity ($\overline{u}$), turbulent fluctuations $\left(u_i' = u_i - \overline{u}_i\right)$, TKE $\left(k_t = 0.5\left(\overline{u'^2} + \overline{v'^2} + \overline{w'^2}\right)\right)$, and Reynolds stress ($-\overline{u'w'}$) were computed for 5-min time segments, where overbar denotes time-averages and prime denotes turbulent fluctuations. Here, we report $\overline{u}$ measured at ~ 0.03 m above the bed by VP1, and ~ 0.03 and ~ 0.11–0.15 m above the top of vegetation by VP2 and VP3, respectively (Supporting Information Table S1). The TKE and Reynolds stress were vertically averaged over the profiling range excluding a region of poor data quality (40–44 and 63–70 mm from the transmitter). As the impact of waves on flow is not the scope of the study, we excluded data from times with possible wave impacts (significant bottom wave orbital velocity, $u_{bs} > 0.02\ \mathrm{m\ s^{-1}}$) from the analysis (8% of measurements; *see* the next section for the determination of wave properties).

Post-processing of data from other instruments

The data from Vectors were processed using the same procedure for the VPs described above to derive the time-averaged streamwise velocity and Reynolds stress for 5-min segments. We used those flow quantities for determining the bed roughness length (z_0, m) at the site. Specifically, we used the data from the Vector deployed in front of the sparse patch during ebb tide (hence the Vector is located upstream of the patch), which yielded $z_0 = 0.23 \times 10^{-3}$ m and $z_0 = 0.12 \times 10^{-3}$ m for Experiments 1 and 2, respectively (*see* Supporting Information Text S1 for detailed procedure).

The data from ADCPs were processed to remove low-quality data (correlations < 60%) with gaps filled by polynomial interpolation to derive the time-averaged streamwise velocity for each 5-min segment. We used those velocity profiles to estimate the depth- and time-averaged streamwise velocity above the bare bed upstream of the patch (U_{bare}). Specifically, the data from the Signature during flood tides (~ 5 m upstream from the patches) and an Aquadopp during ebb tides (~ 7.5 m upstream from the patches) were used for the estimation of the representative U_{bare} at the site (*see* Supporting Information Text S1 for detailed procedure). The mean flow directions measured by the ADCP upstream from the patches determined the x and y axes orientations for each 5-min segment, which were applied to data from all instruments. Additionally, water depth fluctuations derived from the pressure sensors embedded in the Vectors and ADCPs and the measured atmospheric pressure were used for calculating the H_s and u_{bs}, following the method described in Wiberg and Sherwood (2008) (eqs. 4, 8 in their paper).

Testing of analytical models

We tested an analytical model for near-bed TKE in a channel with rigid, emergent cylindrical-shaped vegetation from previous studies (e.g., Yang et al. 2016; Yang and Nepf 2019) as a predictor for near-bed TKE inside a patch of vegetation. Yang and Nepf (2019) expressed the near-bed TKE (k_t, $\mathrm{m^2\ s^{-2}}$) as a linear combination of bed-generated TKE ($k_{t,\mathrm{bed}}$) and vegetation-generated TKE ($k_{t,\mathrm{veg}}$), which can be described as:

$$k_t = \underbrace{\frac{C_{\mathrm{bed}}\overline{u}^2}{0.19}}_{k_{t,\mathrm{bed}}} + \underbrace{\delta_k\left[\frac{C_{\mathrm{D,form}} n_{\mathrm{veg}} d_{\mathrm{veg}} l}{2(1-\phi)}\right]^{2/3}\overline{u}^2}_{k_{t,\mathrm{veg}}} \quad (1)$$

where C_{bed} is the bed drag coefficient, δ_k is a scale constant, C_{D} is the form drag coefficient of vegetation, n_{veg} is vegetation density ($\mathrm{m^{-2}}$), d_{veg} is vegetation diameter (m), l is the eddy length scale (m), ϕ is the solid volume fraction of vegetation ($\phi = \pi n_{\mathrm{veg}} {d_{\mathrm{veg}}}^2/4$). This model requires a condition of Reynolds number, $R_e = \overline{u} d_{\mathrm{veg}}/\upsilon > 120$ (C. Liu and Nepf 2016), where ν is the kinematic viscosity, to ensure generation of turbulent wakes by vegetation. Based on the results of Tanino and Nepf (2008) and King et al. (2012), we used $l = d_{\mathrm{veg}}$ in Eq. 1. We assumed that $C_{\mathrm{D,form}} \approx C_{\mathrm{D}} \approx 1$, where C_{D} is the total vegetation drag coefficient (Nepf 2012). We set $\delta_k = 1$, following Tanino and Nepf (2008) and Xu et al. (2022). The within-patch velocity at approximately $z = 0.03$ m (u_p) measured by VP1 was used for $\overline{u}$ in Eq. 1. C_{bed} was determined using the z_0 estimated for each experiment (*see* Supporting Information Text S1) as $C_{\mathrm{bed}} = \left[\frac{\kappa}{\ln(h/z_0)-1}\right]^2$, where $\kappa = 0.41$ is the von Kármán constant and h is the water depth (m) (Sous and Maticka 2022). Variations in C_{bed} over the measured h, were small ($C_{\mathrm{bed}} = 0.0035$–$0.0065$ and 0.0028–0.0051 for Experiments 1 and 2, respectively). We tested this model for conditions that satisfy $R_e > 120$.

Additionally, we tested analytical models for predicting velocity in submerged canopy spanning the channel width (referred to as two dimensional (2D) canopy model, presented by Z. Chen et al. 2013), and velocity in submerged canopy with finite width (referred to as three dimensional (3D) canopy model, presented by Lei and Nepf 2021). In the 2D canopy model, the water column is partitioned into two layers—a canopy layer ($0 < z < h_{\mathrm{veg}}$) and the overflow layer ($h_{\mathrm{veg}} < z < h$). The flow is assumed to be vertically uniform in each layer, with U_1 in the canopy layer and U_2 in the overflow layer, and the incoming depth-averaged velocity at the bare bed is denoted as U_{bare}. The in-canopy velocity evolves from the leading edge of the canopy. After a distance X_{2D} from the edge (termed the adjustment length), the in-canopy velocity reaches a fully developed condition, referred to as U_{1f}. The U_{1f} normalized by U_{bare} is expressed as:

$$\frac{U_{1f}}{U_{bare}} = \left[1 - \frac{h_{veg}\phi}{h} + \sqrt{\frac{C_D a h_{veg}}{2C_{2D}(1-\phi)}\left(\frac{h-h_{veg}}{h}\right)^3}\right]^{-1} \quad (2)$$

where $a = (n_{veg}d_{veg})$ is the vegetation frontal area per volume (m^{-1}) and C_{2D} is a coefficient that characterizes momentum exchange efficiency between the two layers in a 2D canopy, which is given by $C_{2D} = K_c\left(\frac{\delta}{h}\right)^{1/3}$, where $K_C = 0.07$ is an empirical constant, and δ is the momentum penetration length (m) defined by Nepf and Vivoni (2000). The δ parameter is given by $\delta = \min\left(\frac{0.3}{C_D a}, h - h_{veg}, h_{veg}\right)$, describing the constraints of δ by water surface ($h - h_{veg}$) and vegetation height (h_{veg}). The evolution of in-canopy velocity U_1 from the leading edge ($x = 0$) to the adjustment distance ($x = X_{2D}$) is described as:

$$U_1(x) = U_{1f} + (U_0 - U_{1f})\exp\left(-\frac{3x}{X_{2D}}\right) \quad (3)$$

where U_0 is the canopy-averaged velocity at the leading edge, and X_{2D} is given by Lei and Nepf (2021) as:

$$X_{2D} = \left[3.4 + 2.5\frac{1}{C_D a h_{veg}} - 3.3\left(\frac{h-h_{veg}}{h}\right)^2\right]h_{veg} \quad (4)$$

The 3D canopy model considers a long, rectangular submerged patch, characterized by the stem height h_{veg} and patch width $2b$, and the channel width is defined as $2W$ ($> 2b$). As in the 2D canopy model, the flow is partitioned into two regions—with uniform velocity U_1 inside the canopy and uniform velocity U_2 outside of the canopy. The adjustment length for the 3D canopy is denoted as X_{3D}. Specifically, Lei and Nepf (2021) considered field conditions ($W \gg b$) for application of the model, for which U_{1f} (in-canopy velocity in fully developed conditions) normalized by U_{bare} is expressed as:

$$\frac{U_{1f}}{U_{bare}} = \left[1 + \sqrt{\frac{C_D a b h_{veg}}{2C_{3D}(b+h_{veg})(1-\phi)}}\right]^{-1} \quad (5)$$

where C_{3D} is a coefficient that characterizes momentum exchange efficiency between the canopy region and outer region, which is given by $C_{3D} = K_c\left(\frac{\delta}{R}\right)^{1/3}$, where $K_C = 0.07$, and R is the hydraulic radius ($R \approx h$ under field conditions). The δ is in this case given by $\delta = \min\left(\frac{0.3}{C_D a}, h - h_{veg}, h_{veg}, b\right)$, describing the constraints of δ by water surface, vegetation height, and the half canopy width (b). The evolution of in-canopy velocity U_1 is described by the same equation for the 2D canopy (Eq. 3) with a replacement of the adjustment length with X_{3D}. The X_{3D} is given by Lei and Nepf (2021) as:

$$X_{3D} = \left[3.4 + 2.5\frac{1}{C_D a h_{veg}\frac{b}{b+h_{veg}}} - 3.3\left(\frac{Wh - bh_{veg}}{Wh}\right)^2\right]\left(\frac{bh_{veg}}{b+h_{veg}}\right) \quad (6)$$

where in the field conditions ($W \gg b$), the term $\left(\frac{Wh-bh_{veg}}{Wh}\right)$ approaches to 1, thus Eq. 6 is simplified as:

$$X_{3D} = \left[0.1 + 2.5\frac{1}{C_D a h_{veg}\frac{b}{b+h_{veg}}}\right]\left(\frac{bh_{veg}}{b+h_{veg}}\right) \quad (7)$$

We note that while Lei and Nepf (2021) stated that the 3D canopy model is strictly applicable for b/W and $h_{veg}/h \ll 1$, they demonstrated good performance for $b/W \approx 0.51$ and $h_{veg}/h \approx 0.34$. In our field experiments, the limit of $h_{veg}/h \approx 0.34$ corresponds to a water depth of $h = 0.34$ m for $h_{veg} = 0.1$ m, and $h = 0.68$ m for $h_{veg} = 0.2$ m ($b/W \approx 0$ under field conditions). Note that the water depth dependence of U_{1f}/U_{bare} observed in the 2D canopy model (Eq. 2) is diminished in the limit $b/W \sim 0$ in the 3D canopy model (Eq. 5).

The within-patch flow velocities at the measurement point, U_1 ($x = 0.5$ m) given by Eq. 3, were predicted using the 2D canopy model (Eqs. 2–4) and the 3D canopy model (Eqs. 5, 7, and 3 using X_{3D} for the adjustment length). In both 2D and 3D canopy models, $C_D = 1$ was used. It is known that flow is decelerated to some extent upstream of vegetation patches (Z. Chen et al. 2013), thus $U_0 < U_{bare}$. However, due to the absence of a predictive model for U_0, we assumed $U_0 = U_{bare}$. Lei and Nepf (2021) showed that the 2D and 3D canopy models accurately describe the evolution of U_1 under this assumption for canopies with ah_{veg} up to 1.86 in their flume experiments, which is well above the highest value in our patches ($ah_{veg} = 1.5$; Table 1). However, neither the 2D nor the 3D canopy model fully represents the circular patches examined in our experiments. The 2D canopy model considers channel-spanning vegetation and therefore does not account for flow diversion at the sides of the patches, which may lead to an overestimation of the in-canopy velocity. In contrast, the 3D canopy model represents a long, rectangular submerged patch of finite width and assumes a higher total frontal area than that of a circular patch with the same width, which could lead to underestimation of the in-canopy velocity to some extent. Finally, both models do not consider the impact of bed drag. Thus, the accuracy of model predictions is expected to worsen as vegetation density decreases and the relative contribution of bed drag to the total drag force increases.

Numerical simulations

We used a three-dimensional hydrodynamic model—Regional Ocean Modeling System (ROMS; Shchepetkin and McWilliams 2005) to support findings from the field data. The vegetation module implemented in ROMS (Beudin et al. 2017; Yoshikai et al. 2023) was used to account for the vegetation effects on hydrodynamics. The vegetation module adds the term for vegetation drag in the momentum equations, where the x-direction drag force by rigid cylindrical-shaped vegetation ($F_{veg,u}$, m s^{-2}) is calculated as follows:

$$F_{\mathrm{veg},u}(z)=\frac{1}{2}C_{\mathrm{D}}n_{\mathrm{veg}}d_{\mathrm{veg}}\overline{u}(z)\sqrt{\overline{u}(z)^2+\overline{v}(z)^2}\quad\text{for}\quad z\le h_{\mathrm{veg}}\tag{8a}$$

$$F_{\mathrm{veg},u}(z)=0\quad\text{for}\quad z>h_{\mathrm{veg}}\tag{8b}$$

where we applied $C_{\mathrm{D}}=1$ in our ROMS simulations. The conversion of mean kinetic energy into TKE through the vegetation drag force is implemented in the turbulence closure model in ROMS. In the present study, the $k-\varepsilon$ turbulence closure model was used (Warner et al. 2005). Specifically, the vegetation module considers additional terms representing the production and dissipation of TKE by vegetation-generated wakes in the equations for k (TKE) and ε (dissipation rate). In this model, the stem diameter (d_{veg}) was specified for representing the length scale of wakes (Tanino and Nepf 2008; King et al. 2012). Supporting Information Text S2 provides the detailed formulations of the $k-\varepsilon$ turbulence closure model.

We created a 15 m × 15 m orthogonal grid with 0.1 m horizontal and ∼0.02 m vertical resolution, with a 1 m diameter patch of rigid vegetation at the center of the domain (Supporting Information Fig. S2). Flow was forced at two open lateral boundaries and imposed periodic boundary conditions on the streamwise boundaries. In each model run, we generated a steady unidirectional flow ($U_{\mathrm{bare}}\approx 0.3\,\mathrm{m\,s^{-1}}$) at the bare bed regions well-upstream of the patch. Six scenarios corresponding to field experiments (three vegetation densities and two heights) were simulated (Table 1). For each patch scenario, we simulated flows at different water depths for a total of 60 simulations (Supporting Information Table S2). We then extracted the near-bed velocity at $z\approx 0.03$ m at the center of the patch (u_{p}) for a comparison with field data. However, numerical instabilities occurred in TKE calculations for submerged patches, meaning predictions of TKE were unreliable. We confirmed that near-bed velocity is not sensitive to the magnitude of TKE in our simulations.

We used ROMS simulation results to quantify lateral and vertical deflection of water flux around the patches. For lateral deflection, we defined a transect along the y-axis, perpendicular to the streamwise (x) direction, passing through the patch center and spanning from one edge of the patch to the other edge (transect B–B' in Supporting Information Fig. S2), where the x-coordinate of the patch center is given by $x_{\mathrm{c}}=0.5$ m ($x=0$ at the leading edge). An identical transect was also taken at 4 m upstream of the leading edge (transect A–A' in Supporting Information Fig. S2; $x_{\mathrm{up},L}=-4$ m). The lateral deflection of water flux around the patch ($Q_{\mathrm{def},L}$, $\mathrm{m^3\,s^{-1}}$) is then calculated as the difference between the total water flux through the upstream transect (Q_{up}) and that through the patch transect (Q_{patch}):

$$Q_{\mathrm{def},L}=Q_{\mathrm{up}}-Q_{\mathrm{patch}}=\int_A^{A'}\int_0^h u|_{x=x_{\mathrm{c}}}\,dzdy-\int_B^{B'}\int_0^h u|_{x=x_{\mathrm{up},L}}\,dzdy\tag{9}$$

Note that when vegetation patch is not present, $Q_{\mathrm{up}}=Q_{\mathrm{patch}}$, therefore $Q_{\mathrm{def},L}=0$ (no lateral deflection). Similarly, the vertical deflection of water flux ($Q_{\mathrm{def},V}$, $\mathrm{m^3\,s^{-1}}$) was quantified as the net vertical water flux through a horizontal plane at the height of vegetation ($z=h_{\mathrm{veg}}$). Previous studies on 2D canopies have shown that vertical deflection starts upstream of the patch, but at a distance from the leading edge much less than $X_{2\mathrm{D}}$ (Z. Chen et al. 2013; Zhang et al. 2020). We therefore defined a horizontal plane extending from 0.5 m upstream of the patch leading edge ($x_{\mathrm{up},V}=-0.5$ m) to the patch center (measurement point; x_{c}) in the streamwise direction, and spanning the full width of the patch transect B–B' in the lateral direction. The vertical deflection of water flux ($Q_{\mathrm{def},V}$ $\mathrm{m^3\,s^{-1}}$) was then calculated as:

$$Q_{\mathrm{def},V}=\int_B^{B'}\int_{x_{\mathrm{up},V}}^{x_{\mathrm{c}}} w|_{z=h_{\mathrm{veg}}}\,dxdy\tag{10}$$

Note that $Q_{\mathrm{def},V}$ is not sensitive to the exact location of $x_{\mathrm{up},V}$ (for positions at least a few tens of cm upstream of the patch leading edge).

Results

Vertical flow structure

Figure 2 shows the normalized vertical profiles of time-averaged flow velocities, Reynolds stresses, and TKE measured at the center of the patches (corresponding sample time series are shown in Supporting Information Figs. S3, S4 in Supporting Information Text S3). Measurement data are colored by water depth. The corresponding theoretical profiles for open-channel flows without vegetation are also shown for reference (*see* Supporting Information Text S4 for details). The patch of dense short vegetation (Experiment 1, $h_{\mathrm{veg}}=0.1$ m) showed significant attenuation of velocity, Reynolds stress, and TKE within the patch, but enhanced Reynolds stresses and TKE near the top of the vegetation, relative to profiles for open-channel flows (Fig. 2a–c). The intermediate patch revealed similar profiles albeit with a less pronounced increase in Reynolds stresses and TKE near the top of the vegetation (Fig. 2d–f). Profiles from the sparse patch showed minimal influence of vegetation (Fig. 2g–i). The elevated TKE in the sparse patch for water depth $h>0.4$ m (light green to yellow point) may be due to the local influence of eddies shed from a nearby stem as suggested by the turbulent velocity spectra (*see* Supporting Information Text S5; Supporting Information Fig. S5). Figure 3 shows the comparison of the vertical velocity profiles between the measurements and prediction by ROMS for $h=0.4$ m. The ROMS simulations well reproduced the overall trends of velocity profiles with different vegetation densities and heights.

Near-bed TKE

Figure 4 shows the comparison of measured near-bed TKE and the predicted values using the analytical model (Eq. 1) employing the within-patch velocity measured by VP1 for $\overline{u}$,

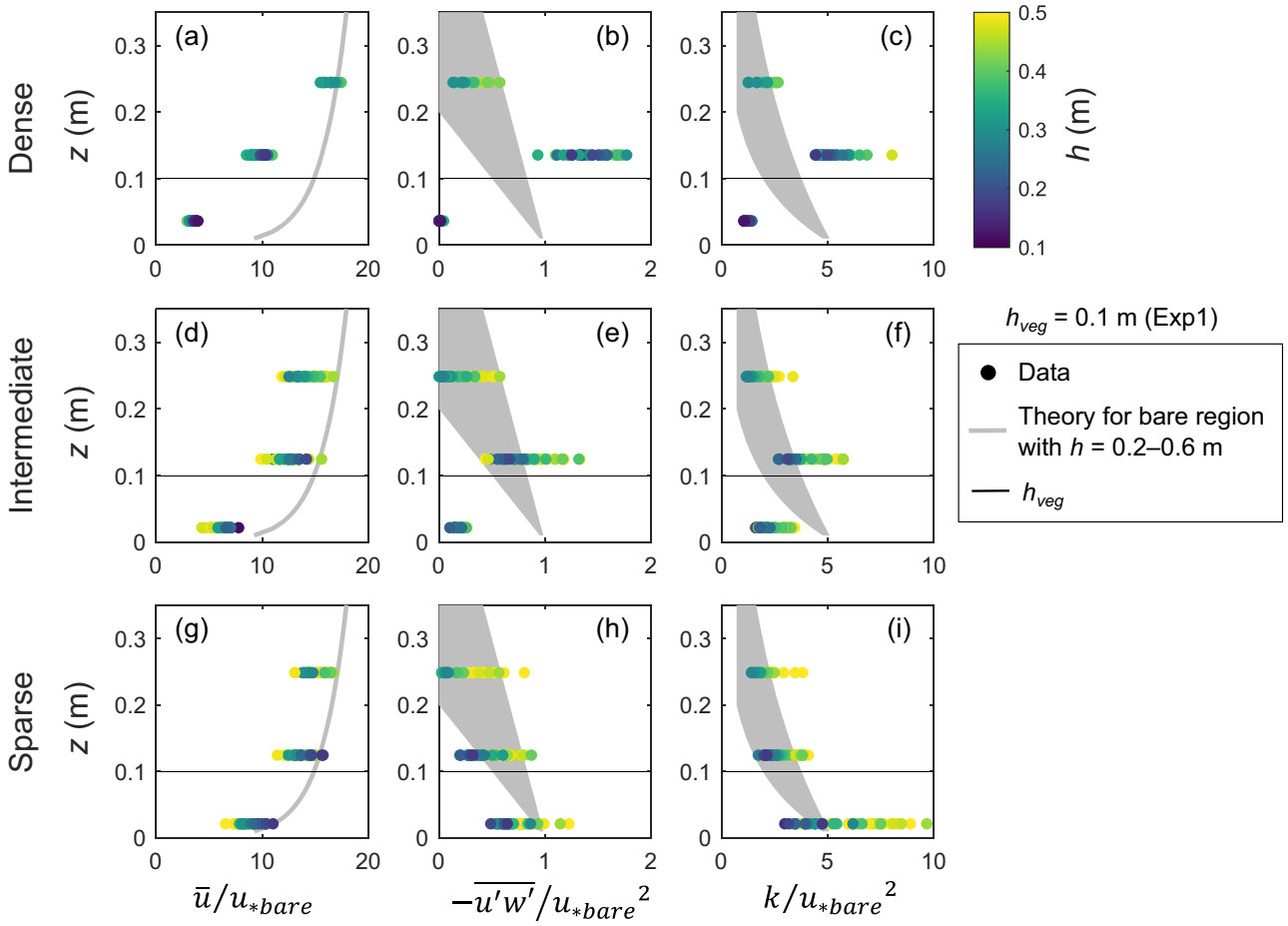

Fig. 2. Time-averaged streamwise velocity ($\bar{u}$), Reynolds stresses ($-\overline{u'w'}$), and TKE (k), normalized using shear velocity at bare bed upstream of the patch ($u_{*\mathrm{bare}}$), measured at three different heights in the (**a**–**c**) dense, (**d**–**f**) intermediate, and (**g**–**i**) sparse patches from Experiment 1 with $h_{\mathrm{veg}} = 0.1$ m. Color bar indicates water depth (h). Gray lines in (**a**, **d**, **g**) show the theoretical velocity profiles for bare sediments. The gray shades in (**b**–**c**, **e**–**f**, **h**–**i**) indicate theoretical profiles for bare sediments for a range of water depths 0.2–0.6 m.

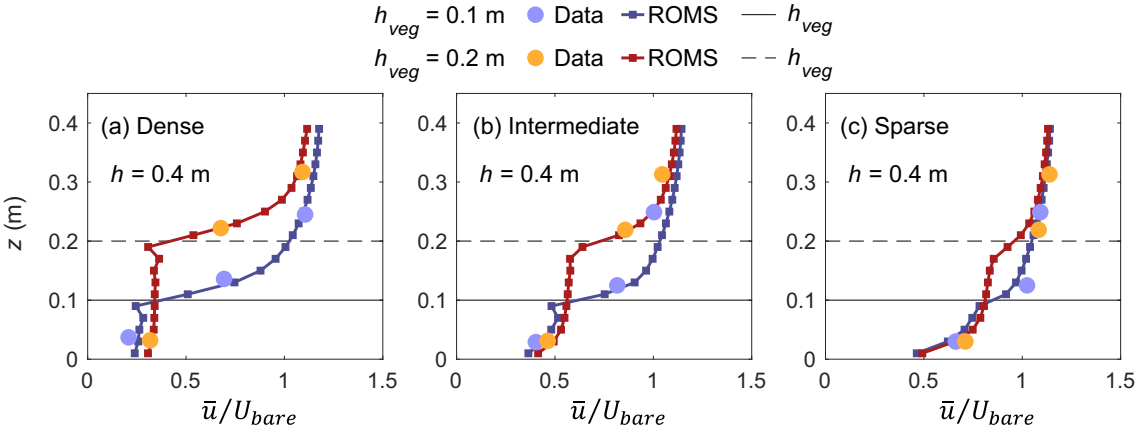

Fig. 3. Comparison of the vertical profiles of $\bar{u}$ at the center of the patch normalized by the depth-averaged in-coming velocity in bare region (U_{bare}) predicted by ROMS with water depth (h) of 0.4 m, and measurements when $h = 0.4$ m for Experiment 1 ($h_{\mathrm{veg}} = 0.1$ m) and Experiment 2 ($h_{\mathrm{veg}} = 0.2$ m) for the (**a**) dense, (**b**) intermediate, and (**c**) sparse patches.

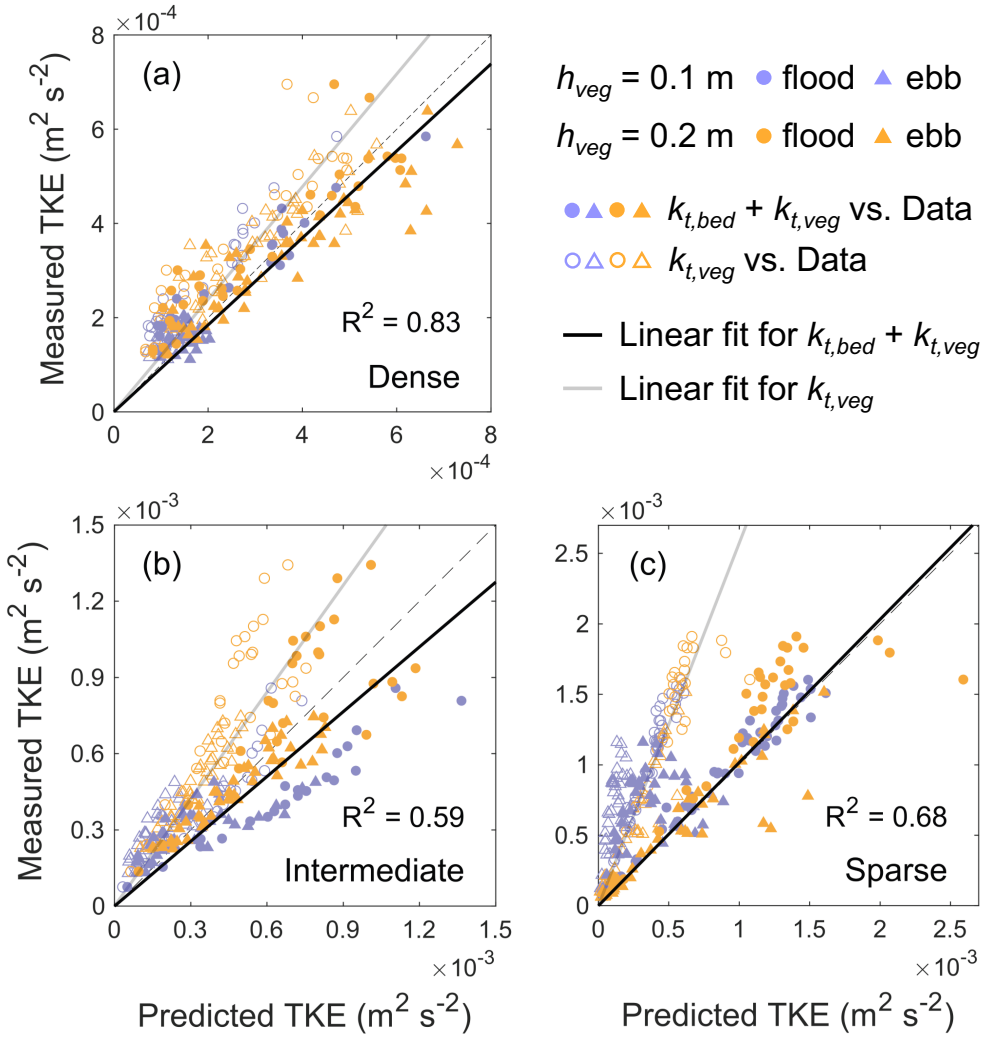

Fig. 4. Predicted vs. measured near-bed TKE in (**a**) dense, (**b**) intermediate, and (**c**) sparse patches with vegetation height $h_{veg} = 0.1$ m (Experiment 1) and $h_{veg} = 0.2$ m (Experiment 2). Bed-generated TKE ($K_{t,bed}$) and vegetation-generated TKE ($k_{t,veg}$) were predicted by Eq. 1 using the measured local velocity at $z = 0.03$ m. R^2 values are provided for the fits to the combined expression. The gray dashed lines indicate the 1 : 1 line.

where the filled symbols represent the sum of bed-generated and vegetation-generated turbulence ($k_{t,bed} + k_{t,veg}$) and the empty symbols represent the $k_{t,veg}$ only. The TKE predicted by Eq. 1 accounting for both components $k_{t,bed}$ and $k_{t,veg}$ showed reasonable agreement with the measured near-bed TKE within the patch for most cases (Fig. 4). The exception is the data from sparse patch for Experiment 1 during ebb tide (filled blue triangles in Fig. 4c), for which predictions significantly underestimated observations (by a factor of $\sim$2.6). These underestimations may be due to the influence of local eddies generated by vegetation stems which may have deviated from the spatial average of flows, a condition assumed in Eq. 1 (Supporting Information Text S5; Supporting Information Fig. S5). Overall, results indicate that near-bed TKE in the patches is a combination of vegetation-generated turbulence ($k_{t,veg}$) and bed-generated turbulence ($k_{t,bed}$) throughout the tidal cycles. For sparser vegetation, the relative importance of $k_{t,bed}$ over $k_{t,veg}$ grows, and accounting for only $k_{t,veg}$ significantly underestimates near-bed TKE (gray line in Fig. 4c).

Effects of variable water depth, vegetation density, and height

For all patches, the normalized within-patch near-bed velocity (u_p/U_{bare}) decreased with water depth (Fig. 5a–c), with smaller u_p/U_{bare} observed for denser patches. Notably, for the same vegetation density, the shorter patch (Experiment 1) showed smaller u_p/U_{bare} than the taller patch (Experiment 2) for a given water depth, despite the smaller total frontal area in the shorter patch than the taller patch. This trend is especially distinct in the dense patches. In contrast, such different trends of velocity between the two vegetation heights were not seen when velocities are compared with the submergence

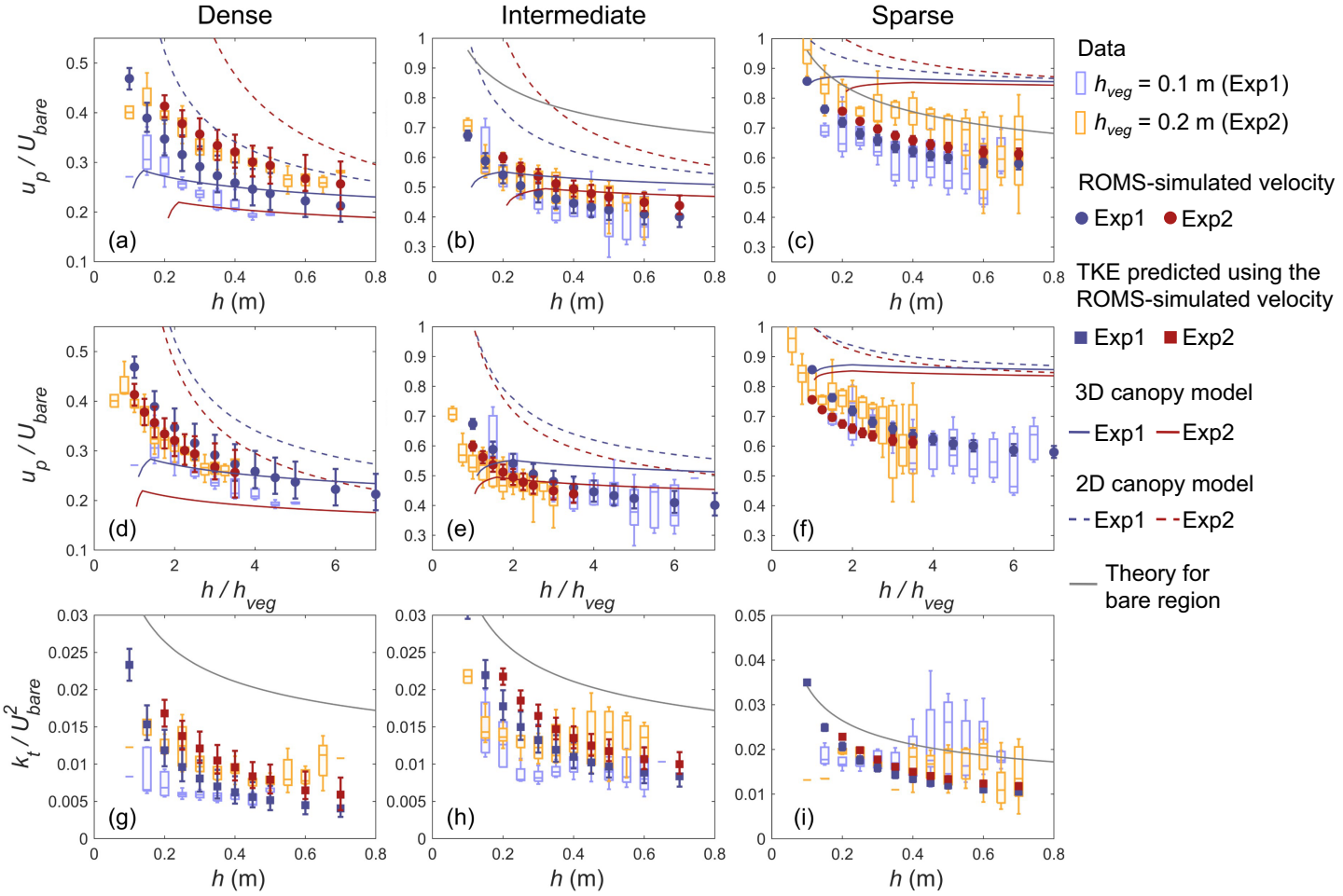

Fig. 5. Within-patch near-bed velocity (u_p) normalized by the depth-averaged incoming velocity in bare region (U_{bare}) as a function of (**a**–**c**) water depth (h), and (**d**–**f**) vegetation submergence ratio (h/h_{veg}). (**g**–**i**) Near-bed turbulent kinetic energy (k_t) normalized by U_{bare}^2 as a function of water depth, for the dense (left column), intermediate (middle column), and sparse (right column) patches. Box plots are data binned into water depths of 0.05 m increments. Symbols show numerical model predictions, with error bars indicating the simulation results at one grid-cell (0.1 m) apart from the center of the patch. In (**g**–**i**) symbols are the k_t predicted by Eq. 1 using the simulated within-patch velocities at $z = 0.03$ m.

ratio (h/h_{veg}) (Fig. 5d–f). The 2D canopy model captured the observed trends in velocities with vegetation height and water depth but significantly overestimated the magnitudes. The 3D canopy model better predicted the velocity magnitude but did not capture the trends. Correspondingly, the 3D canopy model largely underestimated velocity for the tall dense patch (Fig. 5a,d). As expected, both models showed a tendency to overestimate within-patch velocity as vegetation density decreases (particularly for the sparse patches), due to the enhanced relative importance of bed drag compared with vegetation drag, which is not accounted for in the models. In contrast, ROMS simulations well reproduced both trends and magnitude. Although the measured velocities at $z = 0.03$ m (u_p) were compared with the canopy-averaged velocities (U_1) predicted by the 2D and 3D canopy models in Fig. 5, ROMS simulations suggested that the velocity at $z = 0.03$ m provides a good representation of U_1, especially for dense patches. Specifically, for $h = 0.4$ m (results shown in Fig. 3), $u_p/U_{bare} \approx U_1/U_{bare} \approx 0.26$ for the short dense patch, and ≈ 0.33 for the tall dense patch. These results indicate that the discrepancies between the 2D/3D canopy model predictions and measurements were not due to the choice of velocity measurement height.

Owing to the faster flows (larger u_p/U_{bare}) in a taller patch, the normalized TKE (k_t/U_{bare}^2) was generally greater than in a shorter patch for a given water depth, especially for dense patches. For example, for water depths of $h = 0.3$ m, u_p/U_{bare} and k_t/U_{bare}^2 were 37% and 64% larger, respectively, than inside the shorter patch (median values; Fig. 5a,g). Conversely, k_t/U_{bare}^2 consistently decreased with an increase in vegetation density (Fig. 5g–i).

Figure 6 shows the fraction of upstream flux deflected laterally ($R_{def,L} = Q_{def,L}/Q_{up}$), and the ratio of vertical deflection flux to lateral deflection flux ($Q_{def,V}/Q_{def,L}$) as a function of

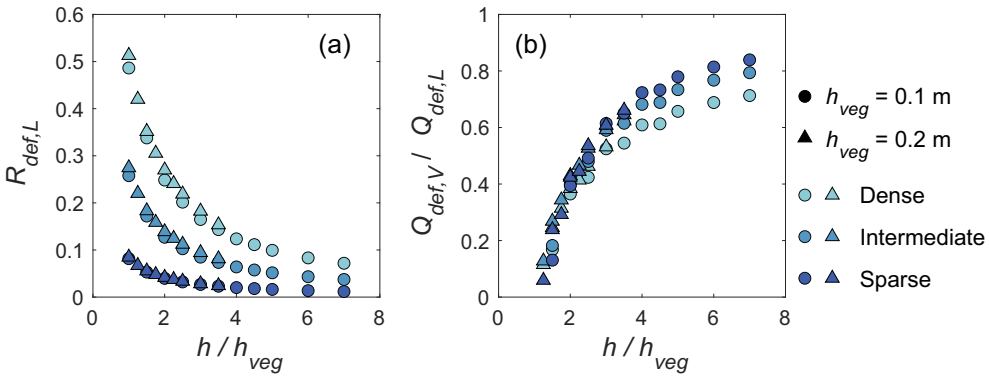

Fig. 6. (**a**) Fraction of water flux deflected laterally around the patches ($R_{\mathrm{def},L}$) and (**b**) ratio of vertical deflection flux ($Q_{\mathrm{def},V}$) to lateral deflection flux ($Q_{\mathrm{def},L}$) as a function of vegetation submergence ratio (h/h_{veg}) calculated using Regional Ocean Modeling System (ROMS) simulation results.

submergence ratio, estimated from ROMS simulation results. The $R_{\mathrm{def},L}$ showed a strong dependence on the vegetation density and submergence ratio, but a minimal dependence on vegetation height (Fig. 6a). As the submergence ratio decreased and approached 1 (emergent condition), $R_{\mathrm{def},L}$ increased, reaching approximately 0.5 for the dense patches and 0.25 for the intermediate patches. $R_{\mathrm{def},L}$ for the sparse patch remained low (< 0.1), suggesting insignificant lateral deflection. The $Q_{\mathrm{def},V}/Q_{\mathrm{def},L}$ also showed a strong dependence on the submergence ratio, but the dependence on vegetation density and height was weak (Fig. 6b). At low submergence ratios (< 2), the vertical deflection was limited compared to lateral deflection ($Q_{\mathrm{def},V}/Q_{\mathrm{def},L} < 0.4$). As the submergence ratio increased, the contribution of vertical deflection became larger, and $Q_{\mathrm{def},V}/Q_{\mathrm{def},L}$ reached $0.6 \sim 0.7$ when $h/h_{\mathrm{veg}} = 4$.

Discussion

We presented high-resolution measurements of flow structures in an artificial patch of vegetation under field conditions, designed to mimic a realistic parameter space of pneumatophores of *Avicennia* spp. mangroves. While previous studies have conducted manipulative field experiments by creating an artificial patch of vegetation (Bouma et al. 2007; Sukhodolova and Sukhodolov 2012), our study provides a first set of detailed observations of mean velocity and TKE within a patch across the whole tide. The key insights are summarized in Fig. 7.

Controls on within-patch near-bed TKE

The significantly increased Reynolds stresses and TKE near the top of the vegetation observed in dense and intermediate patches indicate the formation of a shear layer and coherent vortices (Fig. 2). The shear layer formation is expected in fully developed flows as values for $C_{\mathrm{D}}ah_{\mathrm{veg}}$ (0.75 and 0.25 for dense and intermediate patches, respectively; Table 1) are well above the threshold of shear layer formation ($C_{\mathrm{D}}ah_{\mathrm{veg}} > 0.1$; Nepf et al. 2007). However, the comparable or larger adjustment lengths ($X_{2\mathrm{D}}$ or $X_{3\mathrm{D}}$; Table 1) relative to the distance from the leading edge to the measurement point (0.5 m) indicate that the shear layer was still developing at this location (Z. Chen et al. 2013; Zhang et al. 2020). The penetration length δ—the depth that the shear layer vortices penetrate into the canopy—provides an indication of whether the shear layer vortices are likely to affect near-bed TKE and thereby sediment transport (Nepf et al. 2007; Zhang et al. 2020). For the dense patches in a fully developed condition, δ (0.03–0.05 m; Table 1) is well smaller than the vegetation height, suggesting that the vortices do not penetrate downwards to the bed, consistent with the greatly attenuated Reynolds stresses and TKE near the bed (Fig. 2b,c). In contrast, the penetration length for intermediate short patch ($\delta = 0.08$–0.10 m; Table 1) is comparable to the vegetation height ($h_{\mathrm{veg}} = 0.1$ m), suggesting the potential impact of the shear layer vortices on near-bed TKE in fully developed conditions. However, given that the shear layer was likely in a developing stage at the measurement point, the actual penetration length at this point may have been smaller than that estimated for the fully developed condition. Consequently, the shear layer vortices may not have reached the bed even for the intermediate short patch, as supported by the significantly lowered Reynolds stress and TKE near the bed (Fig. 2e,f). Therefore, in the canopy sublayer—a layer formed below the shear layer—near-bed TKE is mainly attributed to vegetation-generated and bed-generated turbulence with minimal influence from vortices in the shear layer, and predictions from the TKE model of Yang and Nepf (2019) match observations well (Fig. 4a,b). The sparse patch with $C_{\mathrm{D}}ah_{\mathrm{veg}} = 0.06$ did not show the signature of a shear layer, the flow profiles resemble that of open-channel flows (Fig. 2g–i; Nepf 2012). However, because the model of Yang and Nepf (2019) includes the term for bed-generated TKE, the near-bed TKE is predictable even for sparse vegetation (Fig. 4c).

As flow evolves from the leading edge of the patches, the velocity field is spatially non-uniform, leading to non-uniform TKE production in the streamwise (x) direction. Consequently,

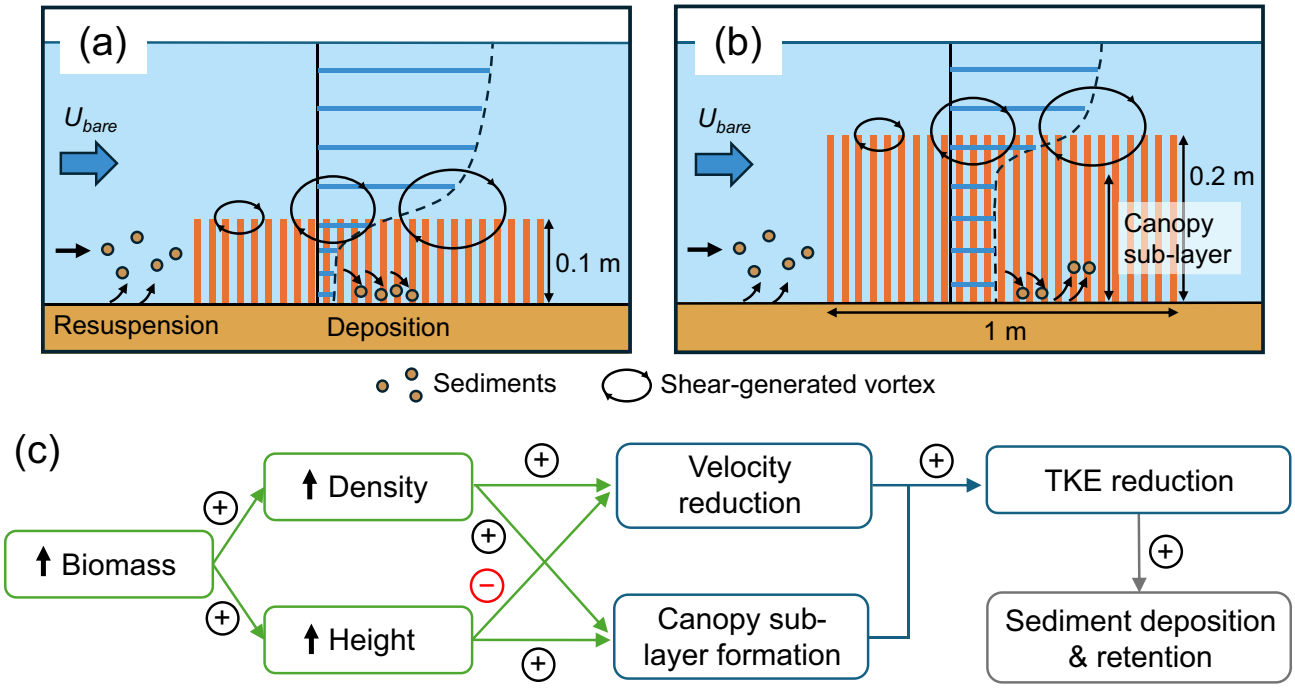

Fig. 7. Schematic summary of the key dependencies of flow structures and sediment transport in a patch with short (**a**) and tall (**b**) vegetation subject to the same hydrodynamic forcing conditions. The schematics are illustrated particularly for patches with dense vegetation that form a distinct shear layer (and correspondingly coherent vortices). Note that patches examined in our experiments were circular. (**c**) A conceptual diagram of the impact of the increase in vegetation density and height following the increase in biomass on sediment deposition and retention inside the patch. A plus sign indicates a positive effect while a minus sign indicates a negative effect.

horizontal advection of TKE generated upstream may influence the TKE-level downstream, in addition to local production/dissipation processes. To examine the impact of horizontal advection, we analyzed ROMS simulation results for an emergent vegetation case with both water depth and vegetation height set to 0.2 m (Runs 34–36; Supporting Information Table S2). For these conditions, TKE at mid-depth ($z = 0.1$ m) is expected to be attributed mostly to vegetation-generated turbulence with limited impact of bed-generated turbulence. The results show that the longitudinal profile of TKE at mid-depth simulated by ROMS is consistent with the prediction of vegetation-generated turbulence (k_{veg}) by Eq. 1 using the local mid-depth velocities from ROMS (Supporting Information Fig. S6). This good agreement indicates that the impact of horizontal advection of TKE is negligible. Hence, the assumption of local equilibrium of TKE production and dissipation in Eq. 1 generally holds, which supports the good performance of Eq. 1 for predicting near-bed TKE within the patches (Fig. 4). Further discussion on the impact of horizontal advection from the perspective of eddy timescale is provided in Supporting Information Text S6.

Effects of vegetation density and height and implications for sediment transport

The 2D canopy model (Eqs. 2–4) was developed by accounting for the flow continuity such that flow diverted out of the canopy is incorporated into the overflow (Z. Chen et al. 2013; Lei and Nepf 2021). The model captured the overall observed trend of u_p/U_{bare}—the significant dependence of u_p/U_{bare} on water depth and the larger u_p/U_{bare} in taller vegetation than shorter vegetation; however, the model largely overestimated the u_p/U_{bare} for all the patches (Fig. 5a–c). The ROMS results suggested significant lateral deflection particularly for the dense and intermediate patches at low submergence ratios ($h/h_{veg} < 2$; Fig. 6a). Such significant lateral deflection explains why the 2D canopy model largely overestimates the within-patch velocity for those patches especially for low submergence ratios. In contrast, the lateral deflection around the sparse patches is generally insignificant ($R_{def,L} < 0.1$; Fig. 6a), and the main cause of the overestimation of within-patch velocity is considered to be the omission of the bed drag term in the model.

Contrary to the 2D canopy model, the 3D canopy model (Eqs. 5–7) developed by Lei and Nepf (2021) considers the finite width of canopy, which is a more realistic representation of the vegetation patches examined in our experiments. The key assumption in the 3D canopy model is that in the field condition where the channel width is considered as infinite, the canopy occupies a small portion of the channel, and hence the flow velocity outside the canopy is considered as uniform and approximately equal to U_{bare} regardless of flow deflection by the canopy. In this condition, the within-patch

velocity is controlled only by canopy drag and the momentum exchange between the canopy region and outer region, and is not constrained by water depth through the flow continuity; the water depth only affects the momentum exchange through the penetration depth δ (*see* the section "Testing of analytical models"). As the vegetation height (h_{veg}) increases, the influence of vegetation drag (the term $C_D abh_{veg}/[2(1-\phi)]$ in Eq. 5) relative to the momentum exchange (the term $C_{3D}(b+h_{veg})$ in Eq. 5) increases, and thus the 3D canopy model predicts slower within-patch velocity. However, our field experiments showed the opposite trend, that is, faster velocity in the taller vegetation patch (Fig. 5a–c). Further, the data showed significant dependence of u_p/U_{bare} on water depth, contrary to the prediction by the 3D canopy model. These trends suggest that the within-patch velocity is significantly influenced by flow continuity even for field conditions; the 3D canopy model that omits flow continuity and assumes the uniform velocities of U_{bare} above and sides of the canopy for the field conditions thus failed to predict u_p/U_{bare}. Instead, the numerical model that explicitly considers the flow deflection at above and sides of the patch as well as the flow continuity reasonably predicted u_p/U_{bare} across patches and water depths.

Water depth controls the space above the patch for flow deflection (a layer of depth $h - h_{veg}$). The observed trend suggests that the reduced space for flow deflection at lower water levels is substantially compensated by the increase in water flux through the patch, leading to greater u_p/U_{bare}. Vegetation height has a similar effect on within-patch velocity—taller vegetation limits the space above the patch for flow deflection and increases water flux through the patch, hence greater u_p/U_{bare}, compared to shorter vegetation, as shown by the data and numerical simulations (Figs. 3, 7a,b). The nearly uniform dependence of u_p/U_{bare} on submergence ratio (h/h_{veg}) for patches with different heights suggests that the impact of both water depth and vegetation height can be represented by a single parameter, submergence ratio (Fig. 5d–f). As a result, our field observations over a smoothly changing water depth unveiled a counter-intuitive effect of vegetation height, for which a taller vegetation patch causes faster flow velocity and hence larger TKE within the canopy despite a larger vegetation frontal area compared with a smaller patch and contrary to the prediction by the 3D canopy model (Figs. 5, 7). This height effect is more significant for the dense patch, due to stronger blockage effects.

Recent laboratory and field studies have emphasized the role of near-bed TKE in controlling bedload transport and sediment movement in vegetated regions (Tinoco and Coco 2014, 2018; Yang and Nepf 2019; Norris et al. 2021). Our results suggest that under conditions of canopy sub-layer formation, vegetation density and height have opposing effects on controlling near-bed TKE, and thus potentially also sediment deposition and retention in a vegetation patch (Fig. 7). The dependence on vegetation height is especially important for sediment transport when water depths become shallow, where changes in relative velocity (u_p/U_{bare}) and relative TKE (k_t/U_{bare}^2) are more sensitive to the change in water depth (or submergence ratio; Fig. 5), and the greatest flow energy and TKE often occur (Supporting Information Figs. S3, S4; e.g., Y. Chen et al. 2016; Mullarney, Henderson, Reyns, et al. 2017; Yoshikai et al. 2022). Hence, the contrasting effects of vegetation density and height may be particularly significant for intertidal vegetation habitats like mangroves and salt marshes where the submergence ratio dynamically changes in diurnal or semidiurnal cycles. Although k_t/U_{bare}^2 is less than that estimated for bare bed conditions (gray curves in Fig. 5g–i), enhancement of TKE by the height effect may lower sedimentation efficiency within a patch. A laboratory study by Gu et al. (2019) found that an increase in submergence ratio (h_{veg}/h) has a negative effect on sedimentation within a patch of vegetation. Our results clarify the mechanisms responsible for this trend—higher submergence ratio increases the within-patch velocity and near-bed TKE, hence reducing sedimentation. Additionally, Nardin and Edmonds (2014) showed that in homogeneous vegetation in a deltaic setting, the largest sedimentation rate occurs for intermediate vegetation heights. Our results similarly imply that for patchy coastal vegetation, an increase in vegetation height may not always enhance within-patch sedimentation. Previous studies have shown that by changing their traits (vegetation density and/or height) vegetation species can alter substrate conditions and these changes vary depending on grain size (van Katwijk et al. 2010; Baaij et al. 2021). Overall, our field experiments strengthen the importance of plant traits (i.e., height vs. density) on biomass allocation in regulating flow and sediment dynamics within vegetation patches (Fig. 7c).

Despite the critical importance of accurate predictions of flow velocity and TKE for a better understanding of geomorphic dynamics in coastal vegetation, our results reveal present analytical models for 2D and 3D canopies are not applicable, suggesting the need for an analytical or parameterized model of velocity deceleration in submerged circular vegetation patches under field conditions. Our ROMS simulations suggest that once the lateral deflection flux is determined based on vegetation density and height (Fig. 6a), the vertical deflection, and hence velocity within the patch, can also be determined through the relationship shown in Fig. 6b. These results can help to develop a parameterized model for flow within patches and to understand how intertidal vegetation alters mean flow and turbulence, promotes sedimentation, and ultimately drives the evolution of vegetated landscapes.

Author Contributions

Masaya Yoshikai: conceptualization, data curation, formal analysis, investigation, methodology, visualization, writing – original draft preparation. Julia C. Mullarney: conceptualization, funding acquisition, investigation, methodology, project

administration, supervision, writing – review and editing. Vinay Nelli: investigation, writing – review and editing. Rémi Chassagne: writing – review and editing. William Nardin: funding acquisition, writing – review and editing. Rafael O. Tinoco: funding acquisition, writing – review and editing.

Acknowledgments

This research is funded by the Royal Society of New Zealand Marsden Fund (Grant 20-UOW-030). The authors gratefully acknowledge Ben Roche and Deonie Castle for their assistance with fieldwork. Open access publishing facilitated by The University of Waikato, as part of the Wiley - The University of Waikato agreement via the Council of Australasian University Librarians.

Conflicts of Interest

None declared.

Data Availability Statement

The field experiment data used in this study are openly available in Zenodo at https://doi.org/10.5281/zenodo.19583886.

References

Baaij, B. M., J. Kooijman, J. Limpens, R. J. C. Marijnissen, and J. M. van Loon-Steensmaet. 2021. "Monitoring Impact of Salt-Marsh Vegetation Characteristics on Sedimentation: An Outlook for Nature-Based Flood Protection." *Wetlands* 41: 76. https://doi.org/10.1007/s13157-021-01467-w.

Balke, T., P. C. Klaassen, A. Garbutt, D. van der Wal, P. M. Herman, and T. J. Bouma. 2012. "Conditional Outcome of Ecosystem Engineering: A Case Study on Tussocks of the Salt Marsh Pioneer *Spartina anglica*." *Geomorphology* 153–154: 232–238. https://doi.org/10.1016/j.geomorph.2012.03.002.

Belliard, J. P., O. Gourgue, G. Govers, M. L. Kirwan, and S. Temmerman. 2023. "Coastal Wetland Adaptability to Sea Level Rise: The Neglected Role of Semi-Diurnal vs. Diurnal Tides." *Limnology and Oceanography Letters* 8: 340–349. https://doi.org/10.1002/lol2.10298.

Beudin, A., T. S. Kalra, N. K. Ganju, and J. C. Warner. 2017. "Development of a Coupled Wave-Flow-Vegetation Interaction Model." *Computers & Geosciences* 100: 76–86. https://doi.org/10.1016/j.cageo.2016.12.010.

Bouma, T. J., S. Temmerman, L. A. van Duren, et al. 2013. "Organism Traits Determine the Strength of Scale-Dependent Bio-geomorphic Feedbacks: A Flume Study on Three Intertidal Plant Species." *Geomorphology* 180–181: 57–65. https://doi.org/10.1016/j.geomorph.2012.09.005.

Bouma, T. J., L. A. Van Duren, S. Temmerman, et al. 2007. "Spatial Flow and Sedimentation Patterns within Patches of Epibenthic Structures: Combining Field, Flume and Modelling Experiments." *Continental Shelf Research* 27: 1020–1045. https://doi.org/10.1016/j.csr.2005.12.019.

Bricker, J. D., and S. G. Monismith. 2007. "Spectral Wave-Turbulence Decomposition." *Journal of Atmospheric and Oceanic Technology* 24: 1479–1487. https://doi.org/10.1175/JTECH2066.1.

Bryan, K. R., W. Nardin, J. C. Mullarney, and S. Fagherazzi. 2017. "The Role of Cross-Shore Tidal Dynamics in Controlling Intertidal Sediment Exchange in Mangroves in Cù Lao Dung, Vietnam." *Continental Shelf Research* 147: 128–143. https://doi.org/10.1016/j.csr.2017.06.014.

Cai, X., Q. Qin, J. Shen, and Y. J. Zhang. 2022. "Bifurcate Responses of Tidal Range to Sea-Level Rise in Estuaries With Marsh Evolution." *Limnology and Oceanography Letters* 7: 210–217. https://doi.org/10.1002/lol2.10256.

Chen, Y., Y. Li, T. Cai, C. Thompson, and Y. Li. 2016. "A Comparison of Biohydrodynamic Interaction Within Mangrove and Saltmarsh Boundaries." *Earth Surface Processes and Landforms* 41: 1967–1979. https://doi.org/10.1002/esp.3964.

Chen, Z., C. Jiang, and H. Nepf. 2013. "Flow Adjustment at the Leading Edge of a Submerged Aquatic Canopy." *Water Resources Research* 49: 5537–5551. https://doi.org/10.1002/wrcr.20403.

Chen, Z., A. Ortiz, L. Zong, and H. Nepf. 2012. "The Wake Structure Behind a Porous Obstruction and Its Implications for Deposition near a Finite Patch of Emergent Vegetation." *Water Resources Research* 48: W09517. https://doi.org/10.1029/2012WR012224.

Cornacchia, L., N. Riviere, J. J. Soundar Jerome, D. Doppler, F. Vallier, and S. Puijalon. 2022. "Flow and Wake Length Downstream of Live Submerged Vegetation Patches: How Do Different Species and Patch Configurations Create Sheltering in Stressful Habitats?" *Water Resources Research* 58: e2021WR030880. https://doi.org/10.1029/2021WR030880.

da Silva, T. D., J. C. Mullarney, C. A. Pilditch, and G. Coco. 2024. "The Interaction Between Vegetation Patchiness and Tidal Flows in a Shortleaf Seagrass Meadow." *Limnology and Oceanography* 69: 2422–2435. https://doi.org/10.1002/lno.12679.

Dahdouh-Guebas, F., J. G. Kairo, R. De Bondt, and N. Koedam. 2007. "Pneumatophore Height and Density in Relation to Micro-Topography in the Grey Mangrove *Avicennia marina*." *Belgian Journal of Botany* 140: 213–221. https://www.jstor.org/stable/20794640.

Dai, W., H. Li, Z. Gong, et al. 2021. "Self-Organization of Salt Marsh Patches on Mudflats: Field Evidence Using the UAV Technique." *Estuarine, Coastal and Shelf Science* 262: 107608. https://doi.org/10.1016/j.ecss.2021.107608.

Diplas, P., C. L. Dancey, A. O. Celik, M. Valyrakis, K. Greer, and T. Akar. 2008. "The Role of Impulse on the Initiation of Particle Movement Under Turbulent Flow Conditions." *Science* 322: 717–720. https://doi.org/10.1126/science.1158954.

Etminan, V., R. J. Lowe, and M. Ghisalberti. 2017. "A New Model for Predicting the Drag Exerted by Vegetation

Canopies." *Water Resources Research* 53: 3179–3196. https://doi.org/10.1002/2016WR020090.

Fagherazzi, S., M. L. Kirwan, S. Mudd, et al. 2012. "Numerical Models of Salt Marsh Evolution: Ecological, Geomorphic, and Climatic Factors." *Reviews of Geophysics* 50: RG1002. https://doi.org/10.1029/2011RG000359.

Furukawa, K., E. Wolanski, and H. Mueller. 1997. "Currents and Sediment Transport in Mangrove Forests." *Estuarine, Coastal and Shelf Science* 44: 301–310. https://doi.org/10.1006/ecss.1996.0120.

Ghisalberti, M., and H. M. Nepf. 2004. "The Limited Growth of Vegetated Shear Layers." *Water Resources Research* 40: W07502. https://doi.org/10.1029/2003WR002776.

Goring, D. G., and V. I. Nikora. 2002. "Despiking Acoustic Doppler Velocimeter Data." *Journal of Hydraulic Engineering* 128: 117–126. https://doi.org/10.1061/(ASCE)0733-9429(2002)128:1(117).

Gu, J., Y. Shan, C. Liu, and X. Liu. 2019. "Feedbacks of Flow and Bed Morphology From a Submerged Dense Vegetation Patch Without Upstream Sediment Supply." *Environmental Fluid Mechanics* 19: 475–493. https://doi.org/10.1007/s10652-018-9633-5.

Horstman, E. M., K. R. Bryan, and J. C. Mullarney. 2021. "Drag Variations, Tidal Asymmetry and Tidal Range Changes in a Mangrove Creek System." *Earth Surface Processes and Landforms* 46: 1828–1846. https://doi.org/10.1002/esp.5124.

King, A. T., R. O. Tinoco, and E. A. Cowen. 2012. "A k–ε Turbulence Model Based on the Scales of Vertical Shear and Stem Wakes Valid for Emergent and Submerged Vegetated Flows." *Journal of Fluid Mechanics* 701: 1–39. https://doi.org/10.1017/jfm.2012.113.

Lei, J., and H. Nepf. 2021. "Evolution of Flow Velocity From the Leading Edge of 2-D and 3-D Submerged Canopies." *Journal of Fluid Mechanics* 916: A36. https://doi.org/10.1017/jfm.2021.197.

Liu, C., and H. Nepf. 2016. "Sediment Deposition Within and Around a Finite Patch of Model Vegetation Over a Range of Channel Velocity." *Water Resources Research* 52: 600–612. https://doi.org/10.1002/2015WR018249.

Liu, D., P. Diplas, J. D. Fairbanks, and C. C. Hodges. 2008. "An Experimental Study of Flow Through Rigid Vegetation." *Journal of Geophysical Research* 113: F04015. https://doi.org/10.1029/2008JF001042.

Liu, M., W. Huai, and B. Ji. 2021. "Characteristics of the Flow Structures Through and Around a Submerged Canopy Patch." *Physics of Fluids* 33: 035144. https://doi.org/10.1063/5.0041782.

Mariotti, G. 2020. "Beyond Marsh Drowning: The Many Faces of Marsh Loss (and Gain)." *Advances in Water Resources* 144: 103710. https://doi.org/10.1016/j.advwatres.2020.103710.

Mariotti, G., and S. Fagherazzi. 2010. "A Numerical Model for the Coupled Long-Term Evolution of Salt Marshes and Tidal Flats." *Journal of Geophysical Research* 115: F01004. https://doi.org/10.1029/2009JF001326.

Mori, N., T. Suzuki, and S. Kakuno. 2007. "Noise of Acoustic Doppler Velocimeter Data in Bubbly Flows." *Journal of Engineering Mechanics* 133: 122–125. https://doi.org/10.1061/(ASCE)0733-9399(2007)133:1(122).

Mudd, S. M., A. D'Alpaos, and J. T. Morris. 2010. "How Does Vegetation Affect Sedimentation on Tidal Marshes? Investigating Particle Capture and Hydrodynamic Controls on Biologically Mediated Sedimentation." *Journal of Geophysical Research* 115: F03029. https://doi.org/10.1029/2009JF001566.

Mullarney, J. C., and S. M. Henderson. 2018. "Flows Within Marine Vegetation Canopies." In Advances in Coastal Hydraulics, edited by V. Panchang and J. Kaihatu, 1–46. World Scientific. https://doi.org/10.1142/9789813231283_0001.

Mullarney, J. C., S. M. Henderson, B. K. Norris, et al. 2017. "A Question of Scale: How Turbulence Around Aerial Roots Shapes the Seabed Morphology in Mangrove Forests of the Mekong Delta." *Oceanography* 30, no. 3: 34–47. https://doi.org/10.5670/oceanog.2017.312.

Mullarney, J. C., S. M. Henderson, J. A. Reyns, B. K. Norris, and K. R. Bryan. 2017. "Spatially Varying Drag Within a Wave-Exposed Mangrove Forest and on the Adjacent Tidal Flat." *Continental Shelf Research* 147: 102–113. https://doi.org/10.1016/j.csr.2017.06.019.

Nardin, W., and D. A. Edmonds. 2014. "Optimum Vegetation Height and Density for Inorganic Sedimentation in Deltaic Marshes." *Nature Geoscience* 7: 722–726. https://doi.org/10.1038/ngeo2233.

Nardin, W., D. A. Edmonds, and S. Fagherazzi. 2016. "Influence of Vegetation on Spatial Patterns of Sediment Deposition in Deltaic Islands During Flood." *Advances in Water Resources* 93: 236–248. https://doi.org/10.1016/j.advwatres.2016.01.001.

Nelli, V., J. C. Mullarney, R. Chassagne, W. Nardin, and R. O. Tinoco. 2026. "Field Measurements and Model Predictions of Turbulent Kinetic Energy in Canopies of Sparse Vegetation Under Tidal Flows." *Limnology and Oceanography Letters* 11: e70096. https://doi.org/10.1002/lol2.70096.

Nepf, H., M. Ghisalberti, B. White, and E. Murphy. 2007. "Retention Time and Dispersion Associated With Submerged Aquatic Canopies." *Water Resources Research* 43: W04422. https://doi.org/10.1029/2006WR005362.

Nepf, H. M. 1999. "Drag, Turbulence, and Diffusion in Flow Through Emergent Vegetation." *Water Resources Research* 35, no. 2: 479–489. https://doi.org/10.1029/1998WR900069.

Nepf, H. M. 2012. "Flow and Transport in Regions With Aquatic Vegetation." *Annual Review of Fluid Mechanics* 44: 123–142. https://doi.org/10.1146/annurev-fluid-120710-101048.

Nepf, H. M., and E. R. Vivoni. 2000. "Flow Structure in Depth-Limited, Vegetated Flow." *Journal of Geophysical Research* 105, no. C12: 28547–28557. https://doi.org/10.1029/2000JC900145.

Norris, B. K., J. C. Mullarney, K. R. Bryan, and S. M. Henderson. 2017. "The Effect of Pneumatophore Density on Turbulence: A Field Study in a *Sonneratia*-Dominated Mangrove Forest, Vietnam." *Continental Shelf Research* 147: 114–127. https://doi.org/10.1016/j.csr.2017.06.002.

Norris, B. K., J. C. Mullarney, K. R. Bryan, and S. M. Henderson. 2021. "Relating Millimeter-Scale Turbulence to Meter-Scale Subtidal Erosion and Accretion Across the Fringe of a Coastal Mangrove Forest." *Earth Surface Processes and Landforms* 46: 573–592. https://doi.org/10.1002/esp.5047.

Ortiz, A. C., A. Ashton, and H. Nepf. 2013. "Mean and Turbulent Velocity Fields Near Rigid and Flexible Plants and the Implications for Deposition." *Journal of Geophysical Research: Earth Surface* 118: 2585–2599. https://doi.org/10.1002/2013JF002858.

Salim, S., C. Pattiaratchi, R. Tinoco, et al. 2017. "The Influence of Turbulent Bursting on Sediment Resuspension Under Unidirectional Currents." *Earth Surface Dynamics* 5: 399–415. https://doi.org/10.5194/esurf-5-399-2017.

Schwarz, C., O. Gourgue, J. van Belzen, et al. 2018. "Self-Organization of a Biogeomorphic Landscape Controlled by Plant Life-History Traits." *Nature Geoscience* 11: 672–677. https://doi.org/10.1038/s41561-018-0180-y.

Schwarz, C., F. van Rees, D. Xie, M. G. Kleinhans, and B. van Maanen. 2022. "Salt Marshes Create More Extensive Channel Networks Than Mangroves." *Nature Communications* 13: 2017. https://doi.org/10.1038/s41467-022-29654-1.

Shchepetkin, A. F., and J. C. McWilliams. 2005. "The Regional Oceanic Modeling System (ROMS): A Split-Explicit, Free-Surface, Topography-Following-Coordinate Oceanic Model." *Ocean Modelling* 9: 347–404. https://doi.org/10.1016/j.ocemod.2004.08.002.

Sous, D., S. Maticka, S. Meul´e, and F. Bouchette. 2022. "Bottom Drag Coefficient on a Shallow Barrier Reef." *Geophysical Research Letters* 49: e2021GL097628. https://doi.org/10.1029/2021GL097628.

Sukhodolova, T. A., and A. N. Sukhodolov. 2012. "Vegetated Mixing Layer Around a Finite-Size Patch of Submerged Plants: 1. Theory and Field Experiments." *Water Resources Research* 48: W10533. https://doi.org/10.1029/2011WR011804.

Tanino, Y., and H. M. Nepf. 2008. "Lateral Dispersion in Random Cylinder Arrays at High Reynolds Number." *Journal of Fluid Mechanics* 600: 339–371. https://doi.org/10.1017/S0022112008000505.

Tinoco, R. O., and G. Coco. 2014. "Observations of the Effect of Emergent Vegetation on Sediment Resuspension Under Unidirectional Currents and Waves." *Earth Surface Dynamics* 2: 83–96. https://doi.org/10.5194/esurf-2-83-2014.

Tinoco, R. O., and G. Coco. 2018. "Turbulence as the Main Driver of Resuspension in Oscillatory Flow Through Vegetation." *Journal of Geophysical Research: Earth Surface* 123: 891–904. https://doi.org/10.1002/2017JF004504.

Tinoco, R. O., J. E. San Juan, and J. C. Mullarney. 2020. "Simplification Bias: Lessons From Laboratory and Field Experiments on Flow Through Aquatic Vegetation." *Earth Surface Processes and Landforms* 45: 121–143. https://doi.org/10.1002/esp.4743.

van Katwijk, M. M., A. R. Bos, D. C. R. Hermus, and W. Suykerbuyk. 2010. "Sediment Modification by Seagrass Beds: Muddification and Sandification Induced by Plant Cover and Environmental Conditions." *Estuarine, Coastal and Shelf Science* 89: 175–181. https://doi.org/10.1016/j.ecss.2010.06.008.

Vandenbruwaene, W., S. Temmerman, T. J. Bouma, et al. 2011. "Flow Interaction with Dynamic Vegetation Patches: Implications for Biogeomorphic Evolution of a Tidal Landscape." *Journal of Geophysical Research* 116: F01008. https://doi.org/10.1029/2010JF001788.

Vovides, A. G., B. Marín-Castro, G. Barradas, U. Berger, and J. López-Portillo. 2016. "A Simple and Cost-Effective Method for Cable Root Detection and Extension Measurement in Estuary Wetland Forests." *Estuarine, Coastal and Shelf Science* 183: 117–122. https://doi.org/10.1016/j.ecss.2016.10.029.

Warner, J. C., C. R. Sherwood, H. G. Arango, and R. P. Signell. 2005. "Performance of Four Turbulence Closure Models Implemented Using a Generic Length Scale Method." *Ocean Modelling* 8: 81–113. https://doi.org/10.1016/j.ocemod.2003.12.003.

Wiberg, P. L., and C. R. Sherwood. 2008. "Calculating Wave-Generated Bottom Orbital Velocities From Surface-Wave Parameters." *Computers & Geosciences* 34: 1243–1262. https://doi.org/10.1016/j.cageo.2008.02.010.

Xu, Y., D. Li, and H. Nepf. 2022. "Sediment Pickup Rate in Bare and Vegetated Channels." *Geophysical Research Letters* 49: e2022GL101279. https://doi.org/10.1029/2022GL101279.

Yang, J. Q., H. Chung, and H. M. Nepf. 2016. "The Onset of Sediment Transport in Vegetated Channels Predicted by Turbulent Kinetic Energy." *Geophysical Research Letters* 43: 11,261–11,268. https://doi.org/10.1002/2016GL071092.

Yang, J. Q., and H. M. Nepf. 2018. "A Turbulence-Based Bed-Load Transport Model for Bare and Vegetated Channels." *Geophysical Research Letters* 45: 10,428–10,436. https://doi.org/10.1029/2018GL079319.

Yang, J. Q., and H. M. Nepf. 2019. "Impact of Vegetation on Bed Load Transport Rate and Bedform Characteristics." *Water Resources Research* 55: 6109–6124. https://doi.org/10.1029/2018WR024404.

Yoshikai, M., T. Nakamura, D. M. Bautista, et al. 2022. "Field Measurement and Prediction of Drag in a Planted *Rhizophora* Mangrove Forest." *Journal of Geophysical Research: Oceans* 127: e2021JC018320. https://doi.org/10.1029/2021JC018320.

Yoshikai, M., T. Nakamura, E. C. Herrera, et al. 2023. "Representing the Impact of *Rhizophora* Mangroves on Flow in a Hydrodynamic Model (COAWST_rh v1. 0): The Importance of Three-Dimensional Root System Structures." *Geoscientific Model Development* 16: 5847–5863. https://doi.org/10.5194/gmd-16-5847-2023.

Yoshikai, M., T. Nakamura, R. Suwa, et al. 2021. "Scaling Relations and Substrate Conditions Controlling the Complexity of *Rhizophora* Prop Root System." *Estuarine, Coastal and Shelf Science* 248: 107014. https://doi.org/10.1016/j.ecss.2020.107014.

Yoshikai, M., T. Nakamura, R. Suwa, R. Rollon, and K. Nadaoka. 2021. "Measurement and Modeling of Above-Ground Root Systems as Attributes of Flow and Wave Attenuation Function of Mangroves." In Mangroves: Ecology, Biodiversity, and Management, edited by R. P. Rastogi, M. Phulwaria, and D. K. Gupta, 279–303. Springer. https://doi.org/10.1007/978-981-16-2494-0.

Zhang, J., J. Lei, W. Huai, and H. Nepf. 2020. "Turbulence and Particle Deposition Under Steady Flow Along a Submerged Seagrass Meadow." *Journal of Geophysical Research: Oceans* 125: e2019JC015985. https://doi.org/10.1029/2019JC015985.

Zong, L., and H. Nepf. 2012. "Vortex Development Behind a Finite Porous Obstruction in a Channel." *Journal of Fluid Mechanics* 691: 368–391. https://doi.org/10.1017/jfm.2011.479.

Supporting Information

Additional Supporting Information may be found in the online version of this article.

Submitted 15 December 2025
Revised 09 May 2026
Accepted 22 May 2026